

Article

# Nucleic acid target sensing using a vibrating sharp-tip capillary and digital droplet loop-mediated isothermal amplification (ddLAMP)

Bethany J. Fike <sup>1</sup>, Kathrine Curtin <sup>1,2</sup> and Peng Li <sup>1,\*</sup><sup>1</sup> C. Eugene Bennett Department of Chemistry, West Virginia University, Morgantown, WV, USA.<sup>2</sup> Department of Mechanical and Aerospace Engineering, West Virginia University, Morgantown, WV, USA

\* Correspondence: Peng.Li@mail.wvu.edu

**Abstract:** Nucleic acid tests are key tools for the detection and diagnosis of many diseases. In many cases, amplification of the nucleic acids is required to reach a detectable level. To make nucleic acid amplification tests more accessible to a point-of-care (POC) setting, isothermal amplification can be performed with a simple heating source. Although these tests are being performed in bulk reactions, the quantification is not as accurate as it would be with digital amplification. Here, we introduce the use of the vibrating sharp-tip capillary for a simple and portable system for tunable on-demand droplet generation. Because of the large range of droplet sizes possible and the tunability of the vibrating sharp-tip capillary, a high dynamic range (~ 2 to 6000 copies/μL) digital droplet loop-mediated isothermal amplification (ddLAMP) system has been developed. It was also noted that by changing the type of capillary on the vibrating sharp-tip capillary, the same mechanism can be used for simple and portable DNA fragmentation. With the incorporation of these elements, the present work paves the way for achieving digital nucleic acid tests in a POC setting with limited resources.

**Keywords:** nucleic acid testing; digital detection; LAMP; DNA fragmentation; POC

**Citation:** To be added by editorial staff during production.

Academic Editor: Firstname Lastname

Received: date

Revised: date

Accepted: date

Published: date



Copyright: © 2024 by the authors. Submitted for possible open access publication under the terms and conditions of the Creative Commons Attribution (CC BY) license (<https://creativecommons.org/licenses/by/4.0/>).

## 1. Introduction

Nucleic acid amplification tests (NAATs) are key tools for the screening, risk assessment, diagnosis, therapy selection, prognosis, and monitoring of many diseases [1]. With the recent COVID-19 pandemic, the need for rapid and accurate nucleic acid testing has been shown in recent years [2-4]. While conventional real time Polymerase Chain Reaction (PCR) [5] methods have demonstrated tremendous success for qualitative analysis as well as semi-quantitative analysis, achieving absolute quantification of target sequences is challenging. The impact of sample matrices and PCR inhibitors often undermines the reliability of copy number quantification. To overcome this limitation, digital PCR was developed, in which the bulk volume is divided into many smaller portions. Each of these portions containing either 0 or 1 copy of the target sequence is then amplified and read individually to determine the “negative” and “positive” portions [6-8]. Absolute quantification is then achieved based on the Poisson distribution. To date, digital PCR has been used in diverse applications including pathogen detection, rare sequence detection, and liquid biopsy.

Despite the tremendous success in laboratory-based tests, developing point-of-care (POC) digital PCR technology has been challenging. To simplify the amplification process and eliminate the need for a thermal cycler, many isothermal amplification methods have been used for digital amplification. Notably, loop-mediated isothermal amplification (LAMP) [9] is the most widely performed reaction due to the high specificity and sensitivity of using loop structures to encourage amplification of the target. To date, many digital LAMP (dLAMP) methods have been reported depending on different mechanisms

for achieving sample compartmentalization. The first class of methods utilize pre-formed or prefabricated structures for distributing bulk samples into small volumes. The use of gel arrays with LAMP reagents embedded inside for amplification has been reported as a possible method for dLAMP [10-13]. Similarly, dLAMP has been performed in commercially available membranes using the pores as a microwell array [14-16]. In addition, Slip-Chip technology [17-23] and self-digitizing microfluidic chips [24-26] have been utilized to integrate additional fluid operations to distribute the bulk solution for dLAMP. In addition to these microwell based dLAMP methods, water-in-oil emulsions (droplets) have also been used for dLAMP due to its advantage of generating a much larger number of individual amplifications with lower cost, termed droplet digital LAMP (ddLAMP). Microfluidic flow focusing and T-junction are the most used methods for generating monodisperse droplets for ddLAMP [27-30]. Although microfluidics-based methods work well for droplet generation, they often require multiple fluid pumps and microfabricated devices making it difficult to be used in POC systems. Non-microfluidic strategies including centrifugal force-based [31-35], inkjet printing [36-39], and electrowetting methods [40] have also been reported to simplify the droplet generation process. However, sophisticated external equipment is still required for operation.

In recent years, droplet generation methods that are simple and portable have been reported. Yuan and colleagues reported a ddLAMP method utilizing a hand-powered droplet generator [41], in which manual syringe based suction pumping is used to form droplets in a microfluidic chip, the droplets are collected in a container and heated with a water bath, and then the droplets are transferred to a well plate for fluorescence imaging. The authors reported a limit of detection of 10 copies per microliter with the system that can be used in POC, however the size of the droplets cannot be tuned so only one average droplet size is possible. Similarly, Wu and colleagues reported a ddLAMP method utilizing microfluidic step-emulsion of droplets through manual pumping of a syringe [42], in which the bacterial DNA targets were distributed into a chip for duplex detection, amplified through using a water bath, and fluorescence imaging. The authors reported a limit of detection of 19.8 copies per microliter. Mao and colleagues reported an open droplet array consisting of hydrophilic and hydrophobic patterning which was sealed with mineral oil, the chip is then incubated, and smartphone-based fluorescent imaging and app-based analysis was performed [43]. The authors have reported a limit of detection of 1 copy of lambda DNA per microliter, however, the method is limited by fixed dimensions of the pattern. Although these simplified droplet generation methods are more POC friendly, the performance of these methods in terms of throughput, monodispersity, and droplet size flexibility is compromised due to the lack of sophisticated control equipment, which leads to reduced analytical performance for digital assays.

Recently, our lab reported a simple and compact droplet generation method based on a vibrating sharp-tip capillary [44]. This system eliminates the need for external pumps and achieves on-demand droplet generation with a portable signal generation, which shows great potential for POC digital nucleic acid tests. In this work, we combine the vibrating sharp-tip capillary droplet generation with LAMP to achieve a simple digital droplet assay for detecting bacteria pathogen sequences. We generated a large range of stable droplet sizes (~0.7 pL to 22 nL) with a single device. We optimized the conditions for the digital LAMP reactions and employed a simple DNA fragmentation method to ensure uniform sample distribution throughout the experiments. Finally, we detected common waterborne pathogens, *Vibrio cholerae* and *Shigella sonnei*, with a linear dynamic range of approximately 2 to 6000 copies/µL. This method eliminates the need for bulky equipment for generating monodisperse droplets and a thermal cycler, which paves the way for a portable and high dynamic range ddLAMP system.

## 2. Materials and Methods

### 2.1 Reservoir preparation

Glass slides (25 x 76 x 1 mm, Fisher Scientific, Pittsburgh, PA) were cut down to the same approximate dimensions as glass cover slides (24 x 60 mm, VWR, Radnor, PA). The cut slides were placed through air plasma treatment, and then placed into a 0.1 M NaOH solution for 1 hour. The slides were then transferred to a hydrophobic coating solution consisting of Octadecyltrimethoxsilane (OTS) (TCI, Portland, OR) (300  $\mu$ L) in Toluene (60 mL) for 2 hours. The slides were then left to air dry propped upright in a fume hood overnight. The glass slides were transferred to Petri dishes and placed in a 60 °C oven. Polydimethylsiloxane (PDMS) solution (SYLGARD™ 184 Silicone Elastomer Kit, DOW, Midland, MI) was prepared 10:1 (polymer to curing agent) and degassed until all air bubbles were removed. PDMS solution was then poured into Petri dishes with Silicon wafers affixed to the bottom. The PDMS was then baked in the same oven for 2 hours. The previously treated glass slides and PDMS were removed from the oven. PDMS was allowed to cool to room temperature, while glass slides were placed into a methanol soak on a shaker. While PDMS slabs were cut to form individual reservoirs, the glass slides were shaken. Once the PDMS slabs were cut, the glass slides were removed from the methanol and rinsed with water and dried with pressurized air. Scotch tape was used to remove any debris from both the PDMS reservoirs and the glass slides. The PDMS and glass slides were air plasma treated and then bonded together. The formed reservoirs were placed back into the oven to finish curing for future use.

## 2.2 Vibrating sharp-tip capillary device preparation

A piezoelectric transducer (4.6 kHz, 27 mm, Murata, Thief River Falls, MN) was attached to a glass cover slide using UV curing glue (Norland Optical Adhesive, Norland, Cranbury, NJ). A weight was used to ensure firm contact between the transducer and slide as well as remove any trapped air bubbles. The glue was cured under a UV lamp for 10 minutes. A pre-pulled glass pipette capillary (TIP20TW1, World Precision Instruments, Sarasota, FL) with a 20- $\mu$ m tip was attached at an angle to the prepared device base using glass glue (Locktite®, Henkel, Rocky Hill, CT). A piece of scotch tape was used to affix the device to storage setup, and the device was labelled with the size of the tip. Each device was then stored by securing the device inside a sealed Petri dish.

The vibrating sharp-tip capillary device for DNA fragmentation was prepared in a similar manner, except for using a PUL-1000 Four-Step Micropipette glass capillary Puller (World Precision Instruments, Sarasota, FL) to pull tips (pre-set program 01) in place of the commercial glass capillary.

## 2.3 Tubing preparation

Lengths of large (0.86 mm I.D. x 1.5 mm O.D.) LDPE tubing (BB31695-PE/6, Scientific Commodities, Inc., Lake Havasu, AZ) approximately 15.2 cm and 30-gauge PTFE tubing (SWTT-30-C, Component Supply, Sparta, TN) approximately 3.8 cm were cut using a razor blade. Each piece of tubing was cleaned using either ethanol or isopropanol. The smaller tubing was inserted into the larger tubing with approximately 19 mm remaining from the end. The tubing connection was sealed using 5-Minute Epoxy (Devcon®, ITW Performance Polymers, Danvers, MA), and the tubing was hung from the benchtop until dry.

## 2.4 DNA Fragmentation

Stock solution of DNA was diluted by 10 times to 50  $\mu$ L in a 200  $\mu$ L microtube. The DNA fragmentation vibrating sharp-tip capillary was checked under the Olympus microscope to ensure the cut tip outer diameter was between 30 and 50  $\mu$ m in diameter. The device was attached to a stand and aligned so that the tip of the device was inserted in the DNA sample. The generator leads were attached to the leads on the piezoelectric transducer, and the signal ran for 30 seconds at 95.0 kHz and 10 Vpp. The DNA is then vortexed for a few seconds to ensure uniform mixing throughout the sample.

## 2.5 ddLAMP reaction

Primer mix was prepared at 10x concentration in the following amounts for 100  $\mu$ L of mix from 100  $\mu$ M stock solutions: 2  $\mu$ L F3, 2  $\mu$ L B3, 4  $\mu$ L Loop F, 4  $\mu$ L Loop B, 16  $\mu$ L FIP, 16  $\mu$ L BIP, and 56  $\mu$ L nuclease-free water. Primer sequences used are listed in the supporting information (Table S1) [45] and were purchased from IDT (Integrated DNA Technologies, Inc., Coralville, IA, USA). LAMP WarmStart® Master mix (E1700, New England Biolabs®, Inc., Ipswich, MA), 10x Primer mix, 20x EvaGreen® Dye in water (#31000, Biotium, Fremont, CA), DNA, and Ambion™ Nuclease-Free Water (AM9938, Invitrogen, Austin, TX) were removed from freezer/refrigerator and warmed to room temperature. The vibrating sharp-tip capillary devices for droplet generation were checked under a microscope to ensure the tips were free from chips, breakages, and blockages. Devices were then cleaned using a small Petri dish of deionized water in a sonicator and a syringe with tubing attached to the device capillary, using the combination of sonication and suction to clean and remove any potential blockages. These devices were then placed in the oven to remove excess water inside the capillary while the LAMP reaction mixture was prepared. Fragmented DNA was diluted using nuclease-free water. The ddLAMP reaction solution was prepared in low-binding 1.7 mL PCR microtubes using the following amounts for final volume of 100  $\mu$ L solution: 50  $\mu$ L 2x WarmStart® LAMP master mix, 10  $\mu$ L 10x Primer mix, 5  $\mu$ L EvaGreen® dye, 4  $\mu$ L DNA (ATCC, Manassas, VA, USA), or water for NTC, and 31  $\mu$ L nuclease-free water. Previously prepared reservoirs were placed onto removable thermal cycler platform and labelled using an ultrafine-tip dry erase marker. Additionally, an extra separate reservoir was prepared to test droplet generation parameters. All reservoirs were filled with 7% (w/v) Gransurf 90 (Grant Industries, Elmwood Park, NJ) in mineral oil (Sigma Aldrich, St. Louis, MO) (3.50 g in 50 mL) with a flat surface corresponding to the top of the reservoir. Syringes were prepared by attaching a 27-gauge needle, gently removing the cap, and introducing approximately 300  $\mu$ L of air to the syringe. The LAMP reaction solution was mixed by pipette before being loaded into the prepared syringe through the needle by suction. The loaded syringe was attached to prepared tubing, which was then attached to the vibrating sharp-tip capillary device for droplet generation. The device was attached to the stand with the capillary parallel to the side of the stand while allowing free movement. The LAMP reaction solution was manually loaded through the tubing into the capillary until a few drops were released from the tip. The syringe was then removed from the tubing, and the tubing was taped in place. The signal generator and amplifier were connected to the leads attached to the piezoelectric transducer on the device. The running frequency and amplitude for the device was adjusted under a microscope until the liquid flow was a steady continuous flow. The droplet generation was then tested by switching the acoustic generator from continuous flow to pulsed signal. After droplet generation for four replicants, the droplets were covered with an overturned Petri dish and a piece of paper to ensure no dust or light entered the reaction reservoirs while the droplets settled into a monolayer (approximately 15 minutes). The reaction reservoirs were loaded into a thermal cycler where LAMP occurred at 65 °C for 1 hour before cooling to 4 °C until ready for imaging. Each droplet field was imaged under a microscope with both bright field and fluorescence images at each position in an "S" pattern until all droplets were imaged.

## 2.6 Image analysis and DNA Counting

Two methods of image analysis were performed using computer software ImageJ (U.S. National Institutes of Health, Bethesda, MD), CellProfiler™ (Broad Institute), and "Define the Rain". With the first analysis method, each image set was analyzed manually. The average droplet diameter of the droplet field was determined with the use of ImageJ. The average droplet diameter was then converted into the average droplet volume. Each bright field image was then analyzed to determine the total number of droplets in the image as well as the full droplet field. Next, each fluorescence image was analyzed to

determine the number of positive droplets in the droplet field. Results for the total number of droplets, the number of positive droplets, and the average droplet volume were collected and used to calculate the copies of DNA target for the individual droplet reservoirs.

In contrast to the manual method, an automated analysis method was also developed. A single bright field image was analyzed using ImageJ to determine the average droplet diameter and the average droplet volume was calculated in the same manner as the manual analysis method. All the fluorescence images for a droplet field were uploaded into the CellProfiler™ software. The software then analyzed the images according to the input parameters. When the software analysis was completed, the resulting fluorescence information was reported as a percentage of the maximum fluorescence intensity possible. As a result, the fluorescence intensity percentages were converted to actual fluorescence intensity values, and these fluorescence intensity values were saved in a “.csv” format. The saved “.csv” file was uploaded into the “Define the Rain” website. The software converted the uploaded data into a histogram and then sorted the values into “negative” and “positive” signal. The total number of reported droplets, the number of reported positive droplets, and the average droplet volume were recorded, and the number of copies of DNA target for the individual droplet reservoirs was calculated.

With both methods, calculating DNA copy number counting was performed using the following equation,

$$C = \frac{-\left(\ln\left(1 - \frac{p}{n}\right)\right)}{V}, \quad (1)$$

in which  $C$  is the calculated DNA copy number,  $p$  is the number of positive droplets,  $n$  is the total number of droplets, and  $V$  is the average droplet volume.

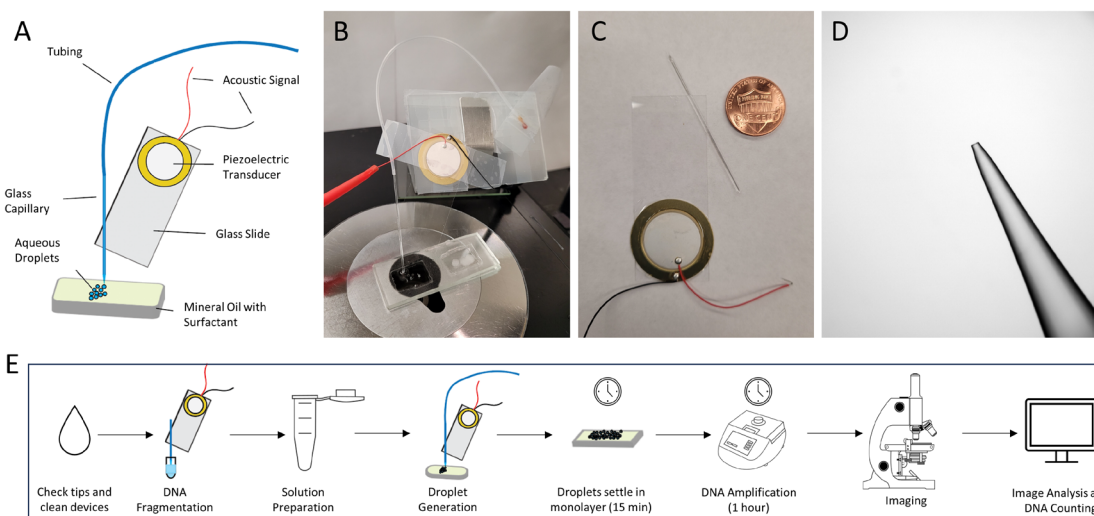


**Figure 1.** The vibrating sharp-tip capillary for droplet generation. (A) Schematic drawing of setup; (B) Real image of setup; (C) Vibrating sharp-tip capillary device with penny for scale; (D) Tip of capillary; (E) Schematic workflow of ddLAMP.

### 3. Results and Discussion

#### 3.1 Droplet Generation using Vibrating Sharp-Tip Capillary

In this work, droplet generation is achieved using a vibrating sharp-tip capillary as shown in Figure 1A. The system is comprised of a glass capillary with a pulled tip, a glass slide, and a piezoelectric transducer. When RF signals are applied to the piezoelectric transducer, oscillating vibration occurring at the tip drives the liquid from the capillary (Figure 2A, Video S1). Due to the strong acoustic streaming induced by the vibrating

sharp-tip, the meniscus between the aqueous and oil phase is compressed to a “triangle” shape, which is sustained by the pumping pressure of the vibrating capillary. When the vibration is stopped, the Laplace pressure will pinch off the liquid at the tip of the capillary. Based on this mechanism, applying pulsed RF signals leads to the generation of highly monodisperse droplets (Figure 2B, Video S2). In this work, the pulsed signal is achieved through amplitude modulation (AM) with a square wave. Due to the simple mechanism of the vibrating sharp-tip capillary, only a low-cost signal generator is needed for droplet generation. In addition, the low power consumption of the device ensures even a battery powered acoustic generator can be used, which allows for a compact and portable method of droplet generation. Another benefit of this droplet generation mechanism is that both droplet number and droplet size can be controlled. Generating various droplet sizes is particularly beneficial to digital PCR assays as the large range of droplet sizes creates a larger dynamic range than would be possible with a single droplet volume possible.

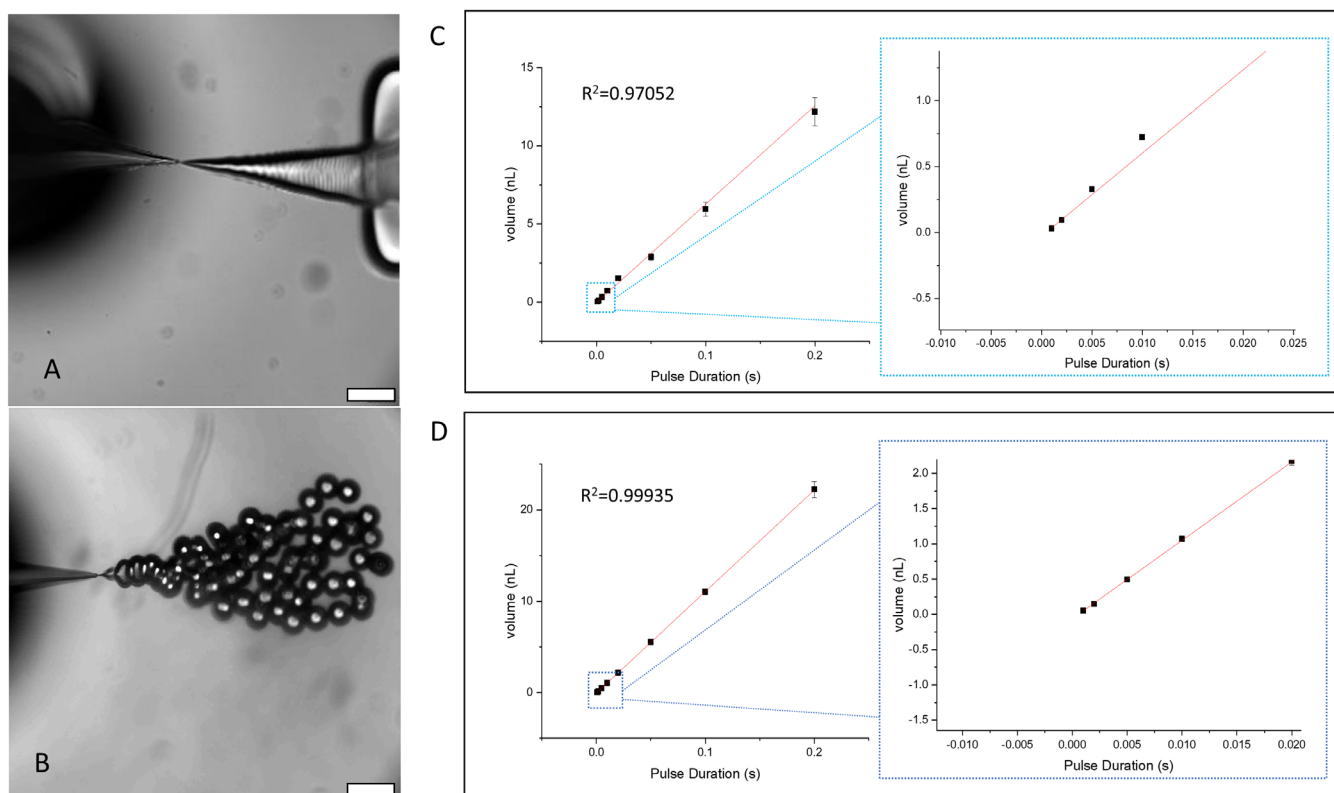


**Figure 2.** Mechanism of droplet generation with the vibrating sharp-tip capillary using continuous flow (A) and pulsed signal (B) modes (Scale bar – 400  $\mu$ m). Linear relationship of droplet volume vs. pulse signal duration using a 20- $\mu$ m tip with expanded view of low pulse durations at 3.5 Vpp (C) and 4.0 Vpp (D).

By working under continuous flow, the device is observed under a microscope and is tuned to its running frequency as each device operates at slightly different parameters. Under the continuous mode, the activation frequency and input voltage are adjusted within the range of 93.0 to 100.0 kHz and 2 to 8 Vpp, activation frequency and input voltage respectively. These parameters are adjusted to ensure a strong and steady continuous flow of liquid from the tip of the capillary. Once the operating frequency and voltage are determined, the acoustic signal is then switched to a pulsed signal for individual droplets to form. The pulsed signal is achieved through amplitude modulation (AM) with a square wave. As a result, when the acoustic signal is “on”, pumping of the liquid occurs from the tip of the device. However, when the acoustic signal is “off”, the pumping of the liquid

stops, and the liquid flow pinches closed allowing for individual droplets to form. Due to the simple mechanism of the vibrating sharp-tip capillary, only an acoustic generator is needed for the pumping mechanism. In addition, the low power consumption of the device ensures even a battery powered acoustic generator can be used, which allows for a compact and portable method of droplet generation. This compact and portable device in conjunction with an isothermal amplification method (LAMP) would increase the accessibility of digital amplification detection of nucleic acids in low resource areas.

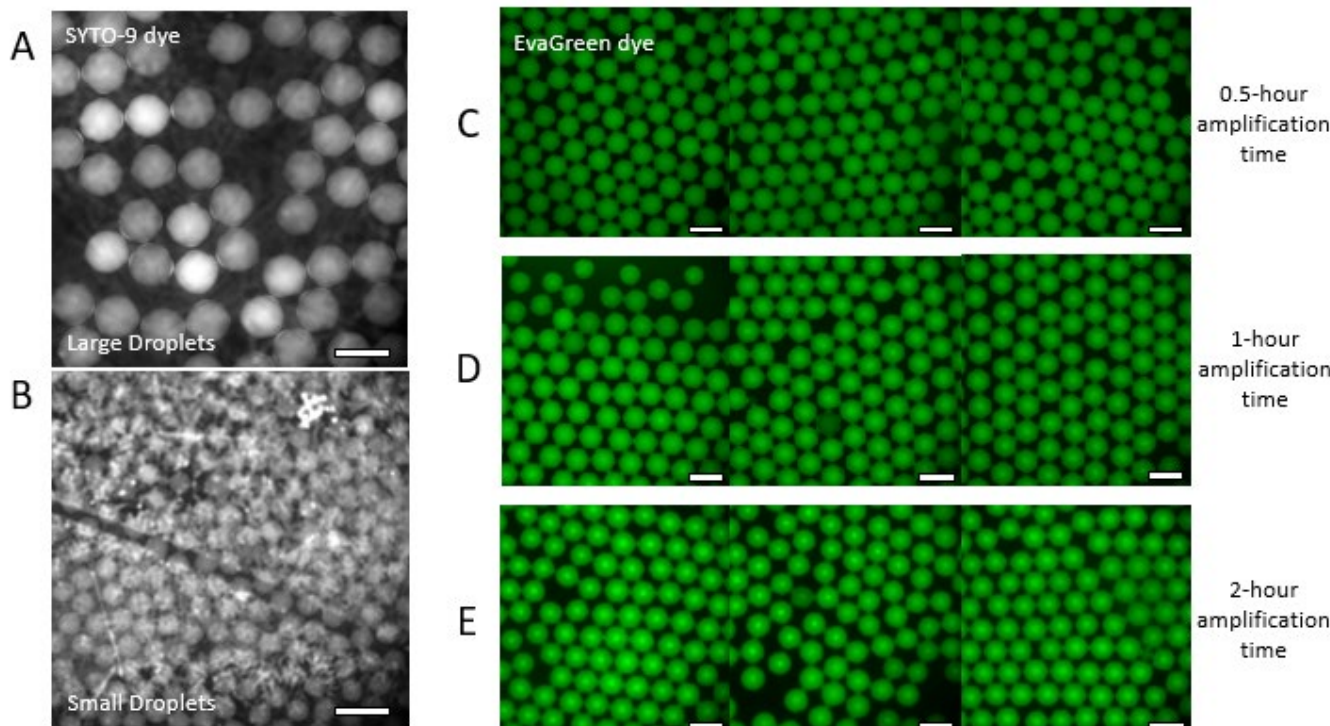


**Figure 3.** Optimization of ddLAMP conditions. Interference of fluorescence signal with using DMSO-based SYTO-9 dye (A and B). Effect of amplification time duration on fluorescence signal (C-E) under same image fluorescence scale. (Scale bar – 200  $\mu$ m)

To tune the droplet size with the vibrating sharp-tip capillary, the input voltage and AM frequency can be adjusted. Under a constant operating frequency and input voltage, the AM frequency can be changed to control the size of the droplets, as shown in Video S3. With a low AM frequency (5 Hz) and long pulse duration (0.2 s), the droplets formed are large in volume. With a high AM frequency (1000 Hz) and short pulse duration (0.001 s), the droplets formed are small in volume. The AM frequency also coordinates to the number of droplets formed per second. The relationship between the average droplet volume and the length of the pulsed signal duration is linear, as shown in the graphs of Figure 2 (C and D), down to a pulsed signal duration of 0.001 seconds. At high AM frequencies (greater than 1000 Hz), the trend shifts from a linear relationship to a plateau, although the vibrating sharp-tip capillary can still perform at these higher pulse frequencies, as shown in Tables S2 and S3. In addition to changing the pulsed signal duration, the droplet volume can be changed by adjusting the input voltage. When the voltage is increased, the droplet volume is also increased due to the increase in the pumping flow rate. This is evident by comparing Figure 2C, in which the input voltage is 3.5 Vpp, and Figure 2D, in which the input voltage is 4.0 Vpp. The higher input voltage (Figure 2D) shows larger droplet volumes than the lower input voltage (Figure 2C). By changing these two parameters, a large range of droplet volumes is possible. With a single device, we have

generated stable droplets of approximately 22 nL (~350  $\mu$ m in diameter) down to approximately 0.7 pL (~11  $\mu$ m in diameter).

### 3.2 Optimization of ddLAMP

Using isothermal nucleic acid amplification would increase accessibility to low resource areas. LAMP was chosen as the isothermal amplification method as it is often used as the “gold standard” for isothermal nucleic acid amplification. Throughout testing, the WarmStart® LAMP kit from New England Biolabs was used. As this kit is typically used for bulk LAMP reactions, optimizations were needed for the ddLAMP reaction. The first optimization necessary was the fluorescent dye as the clear difference in fluorescence intensity is key in identifying negative and positive droplets. With preliminary tests, the SYTO-9 fluorescent dye provided in the WarmStart® LAMP kit and a Listeria monocytogenes bacterial DNA genetic target was used. Because the solvent for the dye is dimethyl sulfoxide (DMSO), there were issues with using this dye. Specifically, since DMSO is an organic solvent, the SYTO-9 dye could leach out of the droplets through the mineral oil and surfactant mixture to adhere to the organically based hydrophobic coating. This adhesion caused optical interference during fluorescent imaging. This phenomenon, shown with larger droplets in Figure 3A, is more prevalent in the smaller droplets, as shown in Figure 3B. Because of the interference from the SYTO-9 dye, it was determined that a water-based fluorescent dye would be necessary. EvaGreen® dye, which is a water-based fluorescent dye, was chosen for use with the ddLAMP protocol.

In addition to the fluorescent dye used, optimization of the optimal amplification time was also necessary. In contrast to bulk detection, with digital detection in droplet the volumes are much smaller in comparison to the bulk reaction and the amount of reagents is limited. Also, each droplet contains a single DNA target, indicating that the exponential amplification will take time to reach a detectable level. For digital detection of amplified nucleic acids, the fluorescence of each individual droplet is detected, and these droplets are then sorted into “negative” and “positive” groups. The key for sorting these droplets is to ensure the amplification has reached its endpoint. For these optimization tests, amplification times of 30-minutes, 1-hour, and 2-hours were used with the same DNA concentration as well as approximately the same droplet size (~145  $\mu$ m in diameter). Although the recommended protocol for the LAMP kit used an amplification time of 30 minutes, there were inconsistencies in the percentage of positive droplets showing up, due to the differences in amplification of each droplet. Additionally, the average fluorescence intensity values of “negative” to “positive” droplets were  $1754 \pm 126$  and  $2189 \pm 152$ , respectively. The 1-hour and 2-hour amplification times were also tested under the same conditions. For the 1-hour amplification time, the average fluorescence intensity values for “negative” and “positive” droplets were  $2199 \pm 130$  and  $2921 \pm 229$ , respectively, while the average fluorescence intensity values of the 2-hour amplification time for “negative” and “positive” droplets were  $2198 \pm 221$  and  $3158 \pm 236$ , respectively. The results of the fluorescence intensity tests are depicted in Figure S1. Because the contrast of fluorescence intensity for “negative” and “positive” droplets of both the 1-hour and 2-hour amplification times were similar, it was determined that a 1-hour amplification time is sufficient for end-point fluorescence measurements of the individual droplets. For all further testing, 1-hour amplification time was used for the ddLAMP protocol.

### 3.3 DNA Fragmentation

During the droplet generation process, genomic DNA strands could settle in the capillary, leading to an increased concentration at the tip region for samples with higher DNA concentrations. This phenomenon affects the uniformity of the amplification results across different droplets. For example, the percentage of positive droplets was lower in the droplets that were generated later in the same experiment. To mitigate this issue, we implemented DNA fragmentation before loading the sample into the vibrating capillary

for droplet generation, which would allow for less settling of the DNA as well as preventing the blocking of the tip of the capillary. Currently, the two most common methods of DNA fragmentation are enzymatic-based and sonication-based fragmentation. With enzymatic-based DNA fragmentation, the enzyme breaks the DNA sequence based on its specific activity, but purification and cleanup of the new ends of the DNA sequence are required for further use making it not as accessible to low resource areas [46]. In contrast, with sonication-based DNA fragmentation, the acoustic waves introduce small gas bubbles into the system which break and cause the DNA to fragment without the need for cleanup, but these instruments are large making them inaccessible [47]. Here, we utilized the vibrating sharp-tip, the same setup as the droplet generation device, to achieve DNA fragmentation [48]. This method allows us to achieve DNA fragmentation without adding additional equipment or procedures, thereby maintaining the low resource requirement for the overall workflow.

346  
347  
348  
349  
350  
351  
352  
353  
354  
355  
356  
357  
358  
359

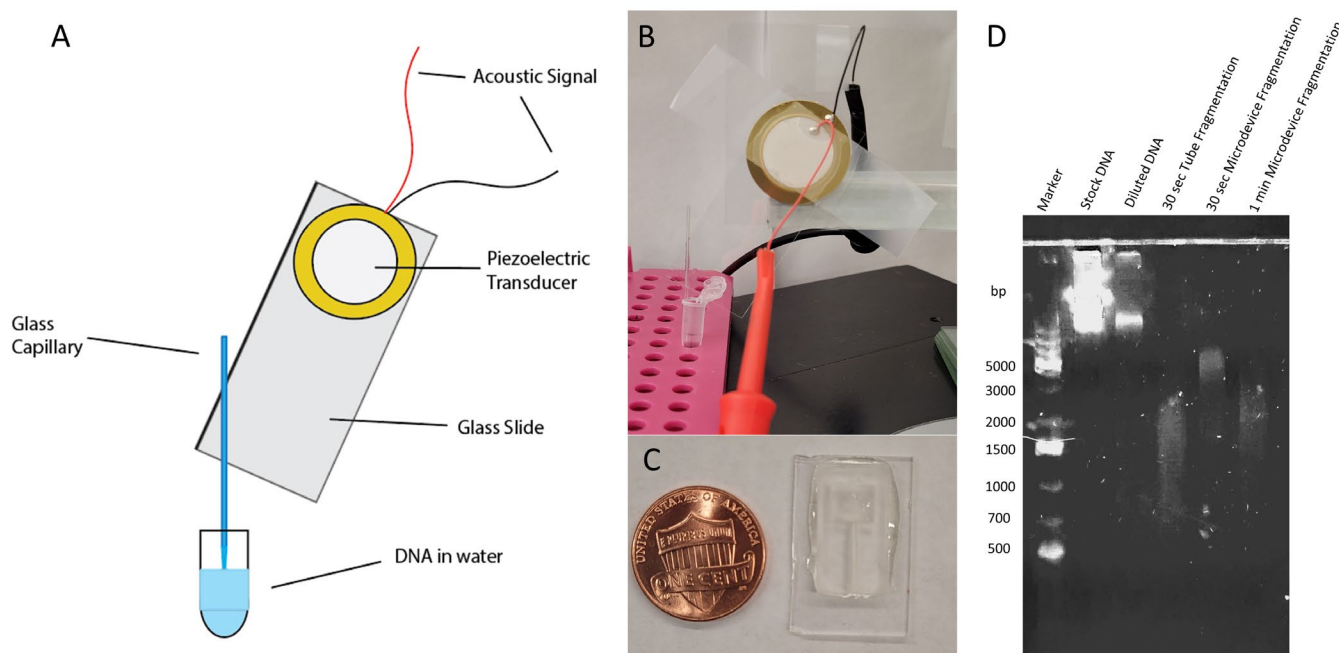


**Figure 4.** The vibrating sharp-tip capillary for DNA Fragmentation. (A) A schematic drawing of the device; (B) A real image of the device; (C) 3D fragmentation microdevice used; (D) Gel electrophoresis results of fragmentation.

360  
361  
362

The setup of the DNA fragmentation device is shown in Figure 4A and B. The capillaries used for the DNA fragmentation device are pulled using a PUL-1000 Four-Step Micro pipette Puller to form a tip with an outer diameter of approximately 35  $\mu$ m. Input parameters of 95.0 kHz activation frequency and a voltage of 10 Vpp were used to break apart the DNA. When the RF signal is applied to the DNA fragmentation device, the vibration of the sharp-tip of the capillary causes strong streaming of the liquid from the single point. This streaming causes fast and strong shearing of the DNA into smaller fragments. Furthermore, the volume of the DNA sample required is only approximately 50  $\mu$ L, which is suitable for processing low volume samples. DNA fragmentation with the vibrating sharp-tip capillary was tested using human male genomic DNA. Three 50  $\mu$ L DNA samples contained in 200  $\mu$ L microtubes were tested for fragmentation. The first sample was fragmented using the vibrating sharp-tip capillary device with the tip submerged in the 50  $\mu$ L sample and acoustics were applied for 30 seconds for fragmentation to occur. The second DNA sample was transferred from the microtube into the 3D printed microdevice (10mm x 18mm x 2 mm), shown in Figure 4C, consisting of an open well

363  
364  
365  
366  
367  
368  
369  
370  
371  
372  
373  
374  
375  
376  
377

(5mm x 6 mm x 1 mm) and an insertion channel for the capillary (radius of 0.6mm for 7mm, followed by a 5° slope decrease for 3 mm). The acoustics were then applied to the capillary for 30 seconds for fragmentation to occur. The third DNA sample was also fragmented within the 3D microdevice, but with acoustics applied for 1 minute. The fragmentation patterns of each of the DNA samples were monitored by agarose gel electrophoresis, shown in Figure 4D. For the gel electrophoresis, three reference solutions were also prepared containing the reference DNA ladder, the pure unfragmented DNA stock, and the diluted unfragmented DNA solution. It was found that the 30-second fragmentation in the microtube produced a range of DNA fragments from approximately 600 to 3000 base pairs. In comparison, the 30-second fragmentation in the 3D microdevice produced a range of DNA fragments from approximately 1500 to 5000 base pairs. In addition, the 1-minute fragmentation in the 3D microdevice produced fragments with a range of approximately 1000 to 4000 base pairs. Based on these results, the vibrating sharp-tip capillary produced the broadest range of DNA fragments in 30 seconds within the microtube. As a result, this setup was used for all further DNA fragmentation required during ddLAMP protocol.

### 3.4 Automated Image Analysis

To improve the image processing time, two image analysis methods, described in length in the Materials and Methods section, were investigated to automate the image processing. First, the image processing was performed manually, as a baseline, to determine the DNA copy numbers for the sample as well as the amount of time necessary. In brief, each of the bright field images are used to determine the average size of the droplets as well as the total number of droplets in the sample reservoir. Each of the fluorescence images are then analyzed for the number of positive droplets contained in the sample reservoir identifying droplets that show an increased fluorescence intensity compared to the dark, negative droplets. The DNA copy number was calculated using the collected values. As the contrast between the fluorescence of the negative and positive droplets is clear, as shown in Figure 5, visual analysis is simple to achieve in a range of droplet sizes down to approximately 65  $\mu$ m in diameter. However, the manual image processing is lengthy, potentially taking hours to complete. In contrast, a fully automated image analysis method was also investigated combining two commercial software platforms, CellProfiler™ [49] and “Define the Rain” [50], and is outlined in Figure S2. In brief, all the fluorescence images for a sample reservoir were uploaded into CellProfiler™, and the individual fluorescent readings of each droplet were recorded according to the input parameters. These fluorescence intensity values were uploaded to the “Define the Rain” website. The website converts the input data into a histogram and then determines the threshold cutoff between negative and positive. The average droplet volume was determined through bright field analysis using ImageJ software. Using the collected values, the DNA copy number could be calculated, and with the automated image analysis, the processing time was reduced to under 15 minutes per sample reservoir. Through comparison of the DNA counts collected from the two different analysis methods, both methods yielded similar results indicating that both methods are viable methods of DNA copy number counting from fluorescence images in instances where the difference in fluorescence intensity is clear.

### 3.5 Quantification Performance of ddLAMP

Finally, we determined the quantification performance and dynamic range of the ddLAMP system, using the waterborne pathogens *Vibrio cholerae* and *Shigella sonnei*. For both bacteria, a DNA genetic target was chosen to be common among all strain types. By using the range of droplet volumes possible, a large dynamic range is possible using ddLAMP. For the *Vibrio cholerae* target, six different concentrations (dilutions) were tested (0.0005x, 0.001x, 0.005x, 0.01x, 0.1x, and 0.875x) with four replicants for each

concentration. The size of the droplets formed was determined based on an estimation of the concentration and the droplet size needed to be within detection range. For example, with the lowest concentration (0.0005x), approximately 500 large droplets with a diameter of approximately 370  $\mu\text{m}$  (~26 nL) were generated and analyzed for determination of the number of DNA copy targets detected in the individual reservoirs. For the highest DNA concentration (0.875x), where approximately 9000 droplets with a diameter of approximately 65  $\mu\text{m}$  (~120 pL) were generated and analyzed for the determination of the number of DNA copy targets detected. Based on the six concentrations and automated image analysis, the *Vibrio cholerae* target has a large linear dynamic range of approximately 2-3700 copies/ $\mu\text{L}$ , as shown in Figure 6A, with an  $R^2$  value of 0.9947. The six concentrations yielded average DNA copy number counts of 2, 6, 23, 46, 360, and 3664 copies/ $\mu\text{L}$  respectively from lowest to highest concentration (reported in Table S4). In addition, the relationship between the calculated DNA copy number counts and the dilution factor is linear, which is visible in the overall graph as well as the expanded view of the lower concentrations. For a comparison, the graph of the manual image analysis is shown in Figure S3 with an  $R^2$  value of 0.9765. In addition, the two analysis methods are plotted together in Figure S4 for a direct comparison.

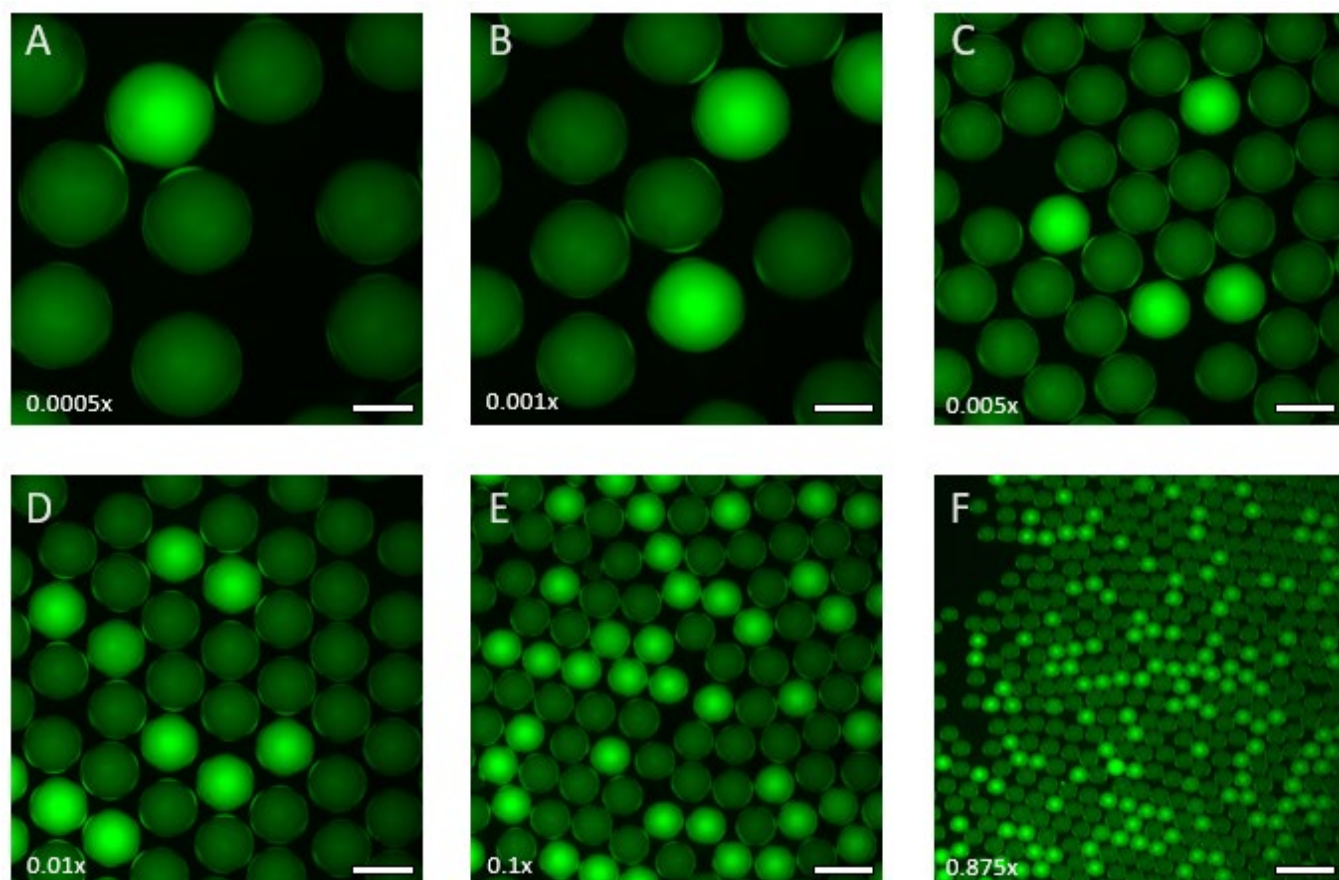


**Figure 5.** Visual representation of ddLAMP at six different concentrations and droplet sizes using *Vibrio Cholerae* as the target. (A) 0.0005x with ~370  $\mu\text{m}$  diameter; (B) 0.001x with ~325  $\mu\text{m}$  diameter; (C) 0.005x with ~190  $\mu\text{m}$  diameter; (D) 0.01x with ~195  $\mu\text{m}$  diameter; (E) 0.1x with ~120  $\mu\text{m}$  diameter; and (F) 0.875x with ~65  $\mu\text{m}$  diameter. (Scale bar – 200  $\mu\text{m}$ )

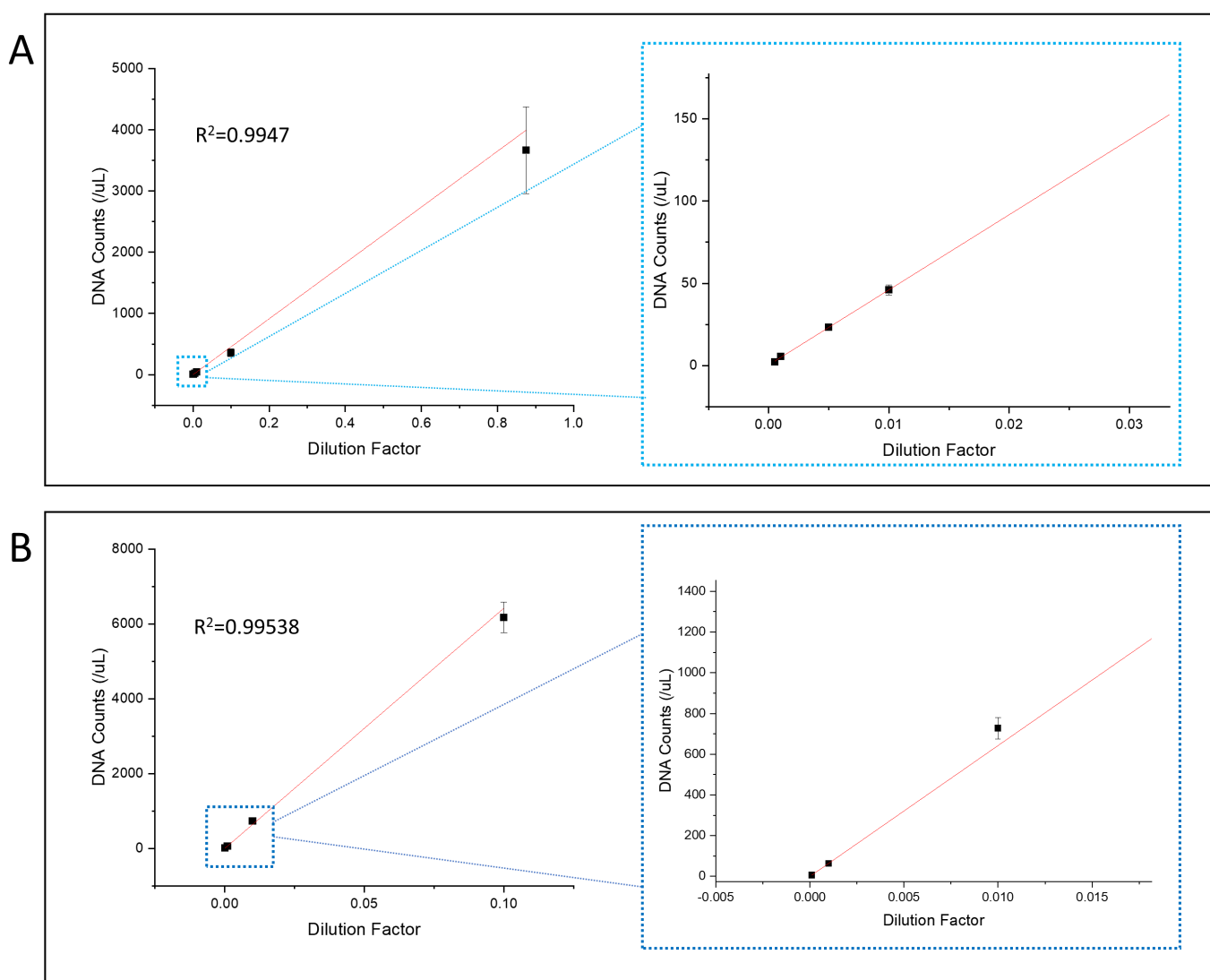


**Figure 6.** Dynamic range of two bacterial strains with expanded view of low concentrations: (A) *Vibrio Cholerae* and (B) *Shigella Sonnei*.

The dynamic range was also tested using *Shigella sonnei* as the genetic target. For this target, only four concentrations (dilutions) were used: 0.0001x, 0.001x, 0.01x, and 0.1x. The testing of the concentrations for *Shigella sonnei* was performed in the same way as with the *Vibrio cholerae*, with four replicants for each of the concentrations. For the lowest concentration (0.0001x), approximately 2000 droplets of 215  $\mu\text{m}$  in diameter (~5.2 nL) were analyzed to calculate the number of gene targets in the reservoirs. In comparison, for the highest concentration (0.1x), approximately 12,000 droplets of 47  $\mu\text{m}$  diameter (~54 pL) were analyzed to calculate the number of gene targets in the reservoirs. The average DNA copy counts were determined to be 7, 63, 727, and 6175 respectively from lowest to highest concentration (reported in Table S5). With these results combined, the *Shigella sonnei* target has a dynamic range of approximately 7-6200 copies/ $\mu\text{L}$ , as shown in Figure 6B with a linear relationship between the calculated DNA copy number and the dilution factor with an  $R^2$  value of 0.99538. The lower limit of the dynamic range can be further improved by using larger sample volumes and better stabilizing of the large droplets. In this study, we kept our sample volume at 100  $\mu\text{L}$ . For lower concentration samples, we could further increase the sample volume to generate more droplets with larger size. As the droplet size increases, it becomes more difficult to maintain the integrity of all droplet populations

during amplification. In future studies, we will explore amplification reactions that occur under milder conditions (e.g., Recombinase Polymerase Amplification) to achieve robust detection with larger droplet sizes.

#### 4. Conclusions

In summary, we have developed a compact, portable, and high dynamic range ddLAMP system that can be used for wide detection of nucleic acids at a POC, or low resource, setting. With a single vibrating sharp-tip capillary, a large range of droplet sizes is possible making a large dynamic range possible. By changing the type of capillary, the same vibrating sharp-tip capillary mechanism can be used for a simple method of DNA fragmentation with low volume consumption of DNA sample. We have also improved the time required for data analysis by automating the image processing and quantification of results. Because of these simple compact, and portable vibrating sharp-tip capillary devices as well as the automation of results, we have reported a high dynamic range ddLAMP system for detecting nucleic acids from approximately 2 to 6000 copies/ $\mu$ L under current conditions. In the present system, both the droplet generation and amplification process are compatible with a portable system. For future studies, we will investigate the possibilities of employing a portable imaging platform to achieve a fully portable digital detection system.

**Supplementary Materials:** The following supporting information can be downloaded at: [www.mdpi.com/xxx/s1](http://www.mdpi.com/xxx/s1); Figure S1: Comparison of fluorescence intensity difference using different reaction time intervals; Figure S2: General overview of CellProfiler image processing; Figure S3: Linear relationship of manual image analysis with expanded view of low concentrations for *Vibrio cholerae*; Figure S4: Comparison of image analysis methods for *Vibrio cholerae*; Table S1: List of primers used; Table S2: Droplet size comparison of a 20- $\mu$ m tip operating at 98.4 kHz and 3.5 Vpp; Table S3: Droplet size comparison of a 20- $\mu$ m tip operating at 98.4 kHz and 4.0 Vpp; Table S4: Data summary of DNA counting methods for *Vibrio cholerae*; Table S5: Data summary of DNA counts at different concentrations for *Shigella sonnei*; Video S1: Continuous flow of liquid from vibrating sharp-tip capillary device; Video S2: Continuous flow and droplet generation from vibrating sharp-tip capillary device; Video S3: On-demand change in droplet volume.

**Author Contributions:** Conceptualization, PL; methodology, BF and KC; formal analysis, BF; resources, BF and KC; writing—original draft preparation, BF; writing—review and editing, PL; visualization, BF; supervision, PL; project funding acquisition, PL. All authors have read and agreed to the published version of the manuscript.

**Funding:** This work was supported by the National Science Foundation (ECCS-2144216).

**Institutional Review Board Statement:** Not applicable

**Data Availability Statement:** The original contributions presented in the study are included in the article/supplementary material, further inquiries can be directed to the corresponding author.

**Conflicts of Interest:** The authors declare no conflicts of interest.

#### References

1. Li, M.; Yin, F.; Song, L.; Mao, X.; Li, F.; Fan, C.; Zuo, X.; Xia, Q. Nucleic Acid Tests for Clinical Translation. *Chem. Rev.* **2021**, *121*, 10469–10558. DOI: 10.1021/acs.chemrev.1c00241.
2. Diego, J. G.-B.; Fernández-Soto, P.; Muro, A. The Future of Point-of-Care Nucleic Acid Amplification Diagnostics after COVID-19: Time to Walk the Walk. *Int. J. Mol. Sci.* **2022**, *23*(22), 14110. DOI: 10.3390/ijms232214110.
3. Fernandes, R. S.; Silva, J. de O.; Gomes, K. B.; Azevedo, R. B.; Townsend, D. M.; Sabino, A. de P.; de Barros, A. L. B. Recent advances in point of care testing for COVID-19 detection. *Biomed. Pharmacother.* **2022**, *153*, 113538. DOI: 10.1016/j.biopha.2022.113538.
4. Kashir, J.; Yaqinuddin, A. Loop mediated isothermal amplification (LAMP) assays as a rapid diagnostic for COVID-19. *Med. Hypotheses.* **2020**, *141*, 109786. DOI: 10.1016/j.mehy.2020.109786.

5. Mullis, K.; Faloona, F.; Scharf, S.; Saiki, R.; Horn, G.; Erlich, H. Specific enzymatic amplification of DNA in vitro: the polymerase chain reaction. *Cold Spring Harb. Symp. Quant. Biol.* **1986**, *51*(1), 263–273. DOI: 10.1101/sqb.1986.051.01.032. 521

6. Curtin, K.; Fike, B. J.; Binkley, B.; Godfrey, T.; Li, P. Recent Advances in Digital Biosensing Technology. *Biosensors.* **2022**, *12*(9), 673. DOI: 10.3390/bios12090673. 523

7. Liu, H.; Lei, Y. A critical review: Recent advances in “digital” biomolecule detection with single copy sensitivity. *Biosens. Bioelectron.* **2021**, *177*, 112901. DOI: 10.1016/j.bios.2020.112901. 525

8. Yin, W.; Zhuang, J.; Li, J.; Xia, L.; Hu, K.; Yin, J.; Mu, Y. Digital Recombinase Polymerase Amplification, Digital Loop-Mediated Isothermal Amplification, and Digital CRISPR-Cas Assisted Assay: Current Status, Challenges, and Perspectives. *Small.* **2023**, *19*(43), 2303398. DOI: 10.1002/smll.202303398. 527

9. Notomi, T.; Okayama, H.; Masubuchi, H.; Yonekawa, T.; Watanabe, K.; Amino, N.; Hase, T. Loop-mediated isothermal amplification of DNA. *Nucleic Acids Res.* **2000**, *28*(12), e63. DOI: 10.1093/nar/28.12.e63. 529

10. Cao, L.; Guo, X.; Mao, P.; Ren, Y.; Li, Z.; You, M.; Hu, J.; Tian, M.; Yao, C.; Li, F.; Xu, F. A Portable Digital Loop-Mediated Isothermal Amplification Platform Based on Microgel Array and Hand-Held Reader. *ACS Sens.* **2021**, *6*(10), 3564–3574. DOI: 10.1021/acssensors.1c00603. 531

11. Chen, C.; Liu, P.; Zhao, X.; Du, W.; Feng, X.; Liu, B.-F. A self-contained microfluidic in-gel loop-mediated isothermal amplification for multiplexed pathogen detection. *Sens. Actuators B: Chem.* **2017**, *239*, 1–8. DOI: 10.1016/j.snb.2016.07.164. 533

12. Huang, X.; Lin, X.; Urmann, K.; Li, L.; Xie, X.; Jiang, S.; Hoffmann, M. R. Smartphone-Based in-Gel Loop-Mediated Isothermal Amplification (gLAMP) System Enables Rapid Coliphage MS2 Quantification in Environmental Waters. *Environ. Sci. Technol.* **2018**, *52*(11), 6339–6407. DOI: 10.1021/acs.est.8b00241. 535

13. Lam, L.; Sakakihara, S.; Ishizuka, K.; Takeuchi, S.; Arata, H. F.; Fujita, H.; Noji, H. Loop-mediated isothermal amplification of a single DNA molecule in polyacrylamide gel-based microchamber. *Biomed. Microdevices.* **2008**, *10*(4), 539–546. DOI: 10.1007/s10544-008-9163-x. 540

14. Lin, X.; Huang, X.; Urmann, K.; Xie, X.; Hoffmann, M. R. Digital Loop-Mediated Isothermal Amplification on a Commercial Membrane. *ACS Sens.* **2019**, *4*(1), 242–249. DOI: 10.1021/acssensors.8b01419. 541

15. Lin, X.; Huang, X.; Zhu, Y.; Urmann, K.; Xie, X.; Hoffmann, M. R. Asymmetric Membrane for Digital Detection of Single Bacteria in Milliliters of Complex Water Samples. *ACS Nano.* **2018**, *12*(10), 10281–10290. DOI: 10.1021/acsnano.8b05384. 543

16. Rolando, J. C.; Jue, E.; Schoepp, N. G.; Ismagilov, R. F. Real-Time, Digital LAMP with Commercial Microfluidic Chips Reveals the Interplay of Efficiency, Speed, and Background Amplification as a Function of Reaction Temperature and Time. *Anal. Chem.* **2019**, *91*(1), 1034–1042. DOI: 10.1021/acs.analchem.8b04324. 544

17. Du, W.; Li, L.; Nichols, K. P.; Ismagilov, R. F. SlipChip. *Lab Chip.* **2009**, *9*(16), 2286–2292. DOI: 10.1039/B908978K. 545

18. Lyu, W.; Zhang, J.; Yu, Y.; Xu, L.; Shen, F. Slip formation of a high-density droplet array for nucleic acid quantification by digital LAMP with a random-access system. *Lab Chip.* **2021**, *21*(16), 3086–3093. DOI: 10.1039/D1LC00361E. 546

19. Rodriguez-Manzano, J.; Karymov, M. A.; Begolo, S.; Selck, D. A.; Zhukov, D. V.; Jue, E.; Ismagilov, R. F. Reading Out Single-Molecule Digital RNA and DNA Isothermal Amplification in Nanoliter Volumes with Unmodified Camera Phones. *ACS Nano.* **2016**, *10*(3), 3102–3113. DOI: 10.1021/acsnano.5b07338. 547

20. Schoepp, N. G.; Schlappi, T. S.; Curtis, M. S.; Butkovich, S. S.; Miller, S.; Humphries, R. M.; Ismagilov, R. F. Rapid pathogen-specific phenotypic antibiotic susceptibility testing using digital LAMP quantification in clinical samples. *Sci. Transl. Med.* **2017**, *9*(410), eaal3693. DOI: 10.1126/scitranslmed.aal3693. 548

21. Yu, M.; Chen, X.; Qu, H.; Ma, L.; Xu, L.; Lv, W.; Wang, H.; Ismagilov, R. F.; Li, M.; Shen, F. Multistep SlipChip for the Generation of Serial Dilution Nanoliter Arrays and Hepatitis B Viral Load Quantification by Digital Loop Mediated Isothermal Amplification. *Anal. Chem.* **2019**, *91*(14), 8751–8755. DOI: 10.1021/acs.analchem.9b01270. 549

22. Yu, Z.; Lyu, W.; Yu, M.; Wang, Q.; Qu, H.; Ismagilov, R. F.; Han, X.; Lai, D.; Shen, F. Self-partitioning SlipChip for slip-induced droplet formation and human papillomavirus viral load quantification with digital LAMP. *Biosens. Bioelectron.* **2020**, *155*, 112107. DOI: 10.1016/j.bios.2020.112107. 550

23. Yu, Z.; Xu, L.; Lyu, W.; Shen, F. Parallel multistep digital analysis SlipChip demonstrated with the quantification of nucleic acid by digital LAMP-CRISPR. *Lab Chip.* **2022**, *22*(16), 2954–2961. DOI: 10.1039/D2LC00284A. 551

24. Kreutz, J. E.; Wang, J.; Sheen, A. M.; Thompson, A. M.; Staheli, J. P.; Dyen, M. R.; Feng, Q.; Chiu, D. T. Self-digitization chip for quantitative detection of human papillomavirus gene using digital LAMP. *Lab Chip.* **2019**, *19*(6), 1035–1040. DOI: 10.1039/C8LC01223G. 552

25. Ma, Y.-D.; Chang, W.-H.; Luo, K.; Wang, C.-H.; Liu, S.-Y.; Yen, W.-H.; Lee, G.-B. Digital quantification of DNA via isothermal amplification on a self-driven microfluidic chip featuring hydrophilic film-coated polydimethylsiloxane. *Biosens. Bioelectron.* **2018**, *99*(15), 547–554. DOI: 10.1016/j.bios.2017.08.026. 553

26. Wang, J.; Staheli, J. P.; Wu, A.; Kreutz, J. E.; Hu, Q.; Wang, J.; Schneider, T.; Fujimoto, B. S.; Qin, Y.; Yen, G. S.; Weng, B.; Shibley, K.; Haynes, H.; Winer, R. L.; Feng, Q.; Chiu, D. T. Detection of 14 High-Risk Human Papillomaviruses Using Digital LAMP Assays on a Self-Digitization Chip. *Anal. Chem.* **2021**, *93*(6), 3266–3272. DOI: 10.1021/acs.analchem.0c04973. 554

27. Ditchendorf, E.; Ahmed, I.; Sepate, J.; Priye, A. A Smartphone-Enabled Continuous Flow Digital Droplet LAMP Platform for High Throughput and Inexpensive Quantitative Detection of Nucleic Acid Targets. *Sensors.* **2023**, *23*(19), 8310. DOI: 10.3390/s23198310. 555

28. Hu, F.; Li, J.; Zhang, Z.; Li, M.; Zhao, S.; Li, Z.; Peng, N. Smartphone-Based Droplet Digital LAMP Device with Rapid Nucleic Acid Isolation for Highly Sensitive Point-of-Care Detection. *Anal. Chem.* **2020**, *92*(2), 2258–2265. DOI: 10.1021/acs.analchem.9b04967. 579

29. Jiang, L.; Lan, X.; Ren, L.; Yang, M.; Wei, B.; Wang, Y. Design of a Digital LAMP Detection Platform Based on Droplet Microfluidic Technology. *Micromachines* **2023**, *14*(5), 1077. DOI: 10.3390/mi14051077. 580

30. Tan, Y.-L.; Huang, A.-Q.; Tang, L.-J.; Jiang, J.-H. Multiplexed droplet loop-mediated isothermal amplification with scorpion-shaped probed and fluorescence microscopic counting for digital quantification of virus RNAs. *Chem. Sci.* **2021**, *12*(24), 8445–8451. DOI: 10.1039/D1SC00616A. 581

31. Jiang, M.; Liao, P.; Sun, Y.; Shao, X.; Chen, Z.; Fei, P.; Wang, J.; Huang, Y. Rotational scan digital LAMP for accurate quantitation of nucleic acids. *Lab Chip* **2021**, *21*(11), 2265–2271. DOI: 10.1039/d1lc00114k. 582

32. Peng, H.; Zhu, M.; Gao, Z.; Liao, C.; Jia, C.; Wang, H.; Zhou, H.; Zhao, J. A centrifugal microfluidic emulsifier integrated with oil storage structures for robust digital LAMP. *Biomed. Microdevices* **2020**, *22*, 18. DOI: 10.1007/s10544-020-0475-9. 583

33. Schuler, F.; Siber, C.; Hin, S.; Wadle, S.; Paust, N.; Zengerle, R.; von Stetton, F. Digital droplet LAMP as a microfluidic app on standard laboratory devices. *Anal. Methods* **2016**, *8*(13), 2750–2755. DOI: 10.1039/C6AY00600K. 584

34. Zhang, W.; Zheng, K.; Ye, Y.; Ji, J.; Cheng, X.; He, S. Pipette-Tip-Enabled Digital Nucleic Acid Analyzer for COVID-19 Testing with Isothermal Amplification. *Anal. Chem.* **2021**, *93*(46), 15288–15294. DOI: 10.1021/acs.analchem.1c02414. 585

35. Zhang, Z.; Cheng, Y.; Li, X.; Chen, L.; Xu, R.; Qi, X.; Shao, Y.; Gao, Z.; Zhu, M. Bent-Capillary-Centrifugal-Driven Monodisperse Droplet Generator with Its Application for Digital LAMP Assay. *Anal. Chem.* **2023**, *95*(5), 3028–3036. DOI: 10.1021/acs.analchem.2c05110. 586

36. Fan, Z.; Sun, Y.; Lin, J.-M. Self-Assembled Inkjet Printer for Droplet Digital Loop-Mediated Isothermal Amplification. *Chemosensors* **2022**, *10*(7), 247. DOI: 10.3390/chemosensors10070247. 587

37. Hu, Y.; Xu, P.; Luo, J.; He, H.; Du, W. Absolute Quantification of H5-Subtype Avian Influenza Viruses Using Droplet Digital Loop-Mediated Isothermal Amplification. *Anal. Chem.* **2017**, *89*(1), 745–750. DOI: 10.1021/acs.analchem.6b03328. 588

38. Lai, X.; Lu, B.; Wu, H.; Pu, Z.; Yu, H.; Li, D. A novel method for generating monodispersed droplet array by inkjet-patterned hydrophilic symbols for controlled reactions. *IEEE Transducers* **2017**, 650–653. 589

39. Xu, P.; Zheng, X.; Tao, Y.; Du, W. Cross-Interface Emulsification for Generating Size-Tunable Droplets. *Anal. Chem.* **2016**, *88*(6), 3171–3177. DOI: 10.1021/acs.analchem.5b04510. 590

40. Thio, S.; K.; Bae, S. W.; Park, S.-Y. Lab on a smartphone (LOS): A smartphone-integrated, plasmonic-enhanced optoelectro-wetting (OEW) platform for on-chip water quality monitoring through LAMP assays. *Sens. Actuators B: Chem.* **2022**, *358*, 131543. DOI: 10.1016/j.snb.2022.131543. 591

41. Yuan, H.; Tian, J.; Chao, Y.; Chien, Y.-S.; Luo, R.-H.; Guo, J.-Y.; Li, S.; Chou, Y.-J.; Shum, H. C.; Chen, C.-F. Hand-Powered Microfluidics for Parallel Droplet Digital Loop-Mediated Isothermal Amplification Assays. *ACS Sens.* **2021**, *6*(8), 2868–2874. DOI: 10.1021/acssensors.1c00184. 592

42. Wu, C.; Liu, L.; Ye, Z.; Gong, J.; Hao, P.; Ping, J.; Ying, Y. TriD-LAMP: A pump-free microfluidic chip for duplex droplet digital loop-mediated isothermal amplification analysis. *Anal. Chim. Acta* **2022**, *1233*, 340513. DOI: 10.1016/j.aca.2022.340513. 593

43. Mao, P.; Cao, L.; Li, Z.; You, M.; Gao, B.; Xie, X.; Xue, Z.; Peng, P.; Yao, C.; Xu, F. A digitalized isothermal nucleic acid testing platform based on a pump-free open droplet array microfluidic chip. *Analyst* **2021**, *146*(22), 6960–6969. DOI: 10.1039/D1AN01373D. 594

44. He, Z.; Wang, J.; Fike, B. J.; Li, X.; Li, C.; Mendis, B. L.; Li, P. A portable droplet generation system for ultra-wide dynamic range digital PCR based on a vibrating sharp-tip capillary. *Biosens. Bioelectron.* **2021**, *191*, 113458. DOI: 10.1016/j.bios.2021.113458. 595

45. Curtin, K.; Wang, J.; Fike, B. J.; Binkley, B.; Li, P. A 3D printed microfluidic device for scalable multiplexed CRISPR-cas12a biosensing. *Biomed. Microdevices* **2023**, *25*, 34. DOI: 10.1007/s10544-023-00675-x. 596

46. Anderson, S. Shotgun DNA sequencing using cloned DNase I-generated fragments. *Nucleic Acids Res.* **1981**, *9*(13), 3015–3027. DOI: 10.1093/nar/9.13.3015. 597

47. Kasoji, S. K.; Pattenden, S. G.; Malc, E. P.; Jayakody, C. N.; Tsuruta, J. K.; Mieczkowski, P. A.; Janzen, W. P.; Dayton, P. A. Cavitation Enhancing Nanodroplets Mediate Efficient DNA Fragmentation in a Bench Top Ultrasonic Water Bath. *PLoS ONE* **2015**, *10*(7), e0133014. DOI: 10.1371/journal.pone.0133014. 598

48. Li, X.; Wang, J.; Curtin, K.; Li, P. Microfluidic continuous flow DNA fragmentation based on a vibrating sharp-tip. *Microfluid. Nanofluid.* **2022**, *26*, 104. DOI: 10.1007/s10404-022-02610-7. 599

49. Lamprecht, M. R.; Sabatini, D. M.; Carpenter, A. E. CellProfiler: free, versatile software for automated biological image analysis. *Biotechniques* **2007**, *42*(1), 71–75. DOI: 10.2144/000112257. 600

50. Defining The Rain: Automatically analysing BioRad's Digital Droplet PCR Output. Available online: <https://define-therain.org.uk/> (accessed on 01-08-2023). 601

**Disclaimer/Publisher's Note:** The statements, opinions and data contained in all publications are solely those of the individual author(s) and contributor(s) and not of MDPI and/or the editor(s). MDPI and/or the editor(s) disclaim responsibility for any injury to people or property resulting from any ideas, methods, instructions or products referred to in the content.

632  
633  
634